




Polarization rotation boosts strong piezoelectric response in the lead-free perovskite ferroelectric $K_{0.5}Na_{0.5}NbO_3$

Zhi Tan ¹, Jie Xing, ^{1,*} Yuting Peng, ² Qiming Zhang, ² and Jianguo Zhu ^{1,†}

¹College of Materials Science and Engineering, Sichuan University, Chengdu 610065, China

²Department of Physics, University of Texas at Arlington, Texas 76019, USA

 (Received 10 November 2020; revised 23 June 2021; accepted 29 June 2021; published 12 July 2021)

Polarization rotation is considered one of the most important intrinsic origins of high piezoelectricity in perovskite ferroelectrics. Such rotation strongly increases the lateral polarization, thus giving rise to the ultrahigh-shear piezoelectric coefficient. The evolution of polarization vector as a function of shear strain in a lead-free perovskite ferroelectric, $K_{0.5}Na_{0.5}NbO_3$ (KNN), is demonstrated using the first-principle calculations. The polarization rotation is found to correlate directly with the shear piezoelectric constant. The larger the rotation angle, the higher the shear piezoelectric constant. The atomic insight reveals the polarization rotation mainly relies on the reorientation of Nb and O atoms along low potential-energy surfaces. We propose the polarization vector is more likely to rotate along the $[111]_{PC} \rightarrow [101]_{PC} \rightarrow [001]_{PC}$ path instead of direct $[111]_{PC} \rightarrow [001]_{PC}$ transition in high-performance lead-free piezoelectric materials with broad thermotropic phase boundaries; thus, the critical role of orthorhombic structure should be emphasized. We hope that this work will inspire future experimental studies for further developing lead-free piezoelectric materials.

DOI: [10.1103/PhysRevB.104.014104](https://doi.org/10.1103/PhysRevB.104.014104)

Perovskite ferroelectric materials have been discovered over 70 y, and have been constructed widely in technical applications in the electronic industry due to their unique electromechanical response [1,2]. The most attractive interest for these materials is ferroelectric phase boundaries, which possess anomalous physical properties. A familiar example of the $Pb(Ti_{1-x}Zr_x)O_3$ system, known as PZT, exhibits a morphotropic phase boundary with excellent piezoelectric performance near the composition of $x = 0.52$ [3]. Owing to the demands of developing green electronic materials, $K_{1-x}Na_xNbO_3$ alloys (KNN) with high Curie temperature ($T_C \sim 300^\circ C$) and good piezoelectricity ($d_{33} \sim 400$ pC/N) have been paid great attention in the past 20 y [4,5]. In this lead-free ABO_3 ferroelectric, the weak interaction between A-site and O atom allows three distinct ferroelectric phases with the rise of temperature as the order of rhombohedral, orthorhombic, and tetragonal (R, O, and T) [6–8]. Generally, the high piezoelectricity in KNN polycrystals can be attributed to the polymorphic phase transition (PPT) shifting downward to room temperature, modulated by the various elements doping [9]. Saito *et al.* first reported the high piezoelectricity ($d_{33} \sim 416$ pC/N) in Li-, Ta-, and Sb-modulated KNN-based textured ceramics with orthorhombic-tetragonal (O-T) phase boundary in 2004 [4]. Subsequently, the rhombohedral-orthorhombic (R-O) and rhombohedral-tetragonal (R-T) phase boundary were successively developed in the KNN system, which allowed the coexistence of multipolarization states with equal energy, hence enhancing the piezoelectric activity [9]. The recent work has established the high piezoelectricity

($d_{33} > 600$ pC/N) in KNN ceramics with PPT phase boundary that can be compared with that of some PZT ceramics [5,10].

Although significant developments have been achieved in KNN-based materials, completely replacing the lead-based materials remains difficult until now. To overcome the great chasm of piezoelectric performance, there are two puzzles that need to be addressed: first, the origin of huge piezoelectric constant; second, which type of ferroelectric phase boundary is the best for developing high-performance KNN-based materials? Unfortunately, there are few theoretical works to elucidate the core of intrinsic high piezoelectricity in the KNN system. Traditionally, the high piezoelectricity is simply attributed to the coexistence of two ferroelectric phases in KNN-based materials, which enable more switchable polarization directions. However, it is weak to elucidate the lower piezoelectricity of KNN-based materials with rhombohedral-orthorhombic phase boundary containing 20 switchable polarization directions. In our recent work, it is found that the orthorhombic KNN crystal has a very high-shear piezoelectric constant d_{15} , which is considered the main contribution of the high piezoelectric performance of KNN ceramics [11]. What is more, unlike the $PbTiO_3$, the d_{15}/d_{33} of pure KNN crystal exceeds 20 [10], exhibiting the typical characteristic of “rotator” [12]. The above result suggests that the polarization rotation may be the intrinsic origin of high piezoelectricity in KNN materials.

To reveal the nature of the high-shear piezoelectric constant, we have performed the first-principle calculations based on the density-functional theory as implemented in the Vienna *Ab initio* Simulation Package (VASP) [13,14] to study the noncollinear shear piezoelectric effect of KNN. A series of continuous shear strain is employed to be applied

*xingjie@scu.edu.cn

†nic0400@scu.edu.cn

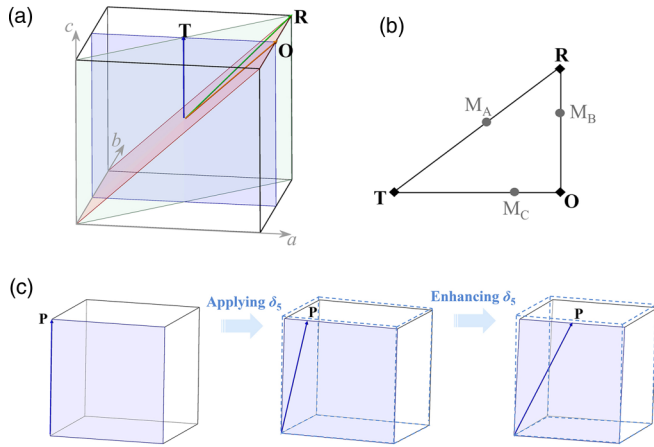


FIG. 1. (a) Schematic illustration for the polarization vectors in perovskite cell. T, O, and R represent the tetragonal, orthorhombic, and rhombohedral structures, respectively. (b) Intersections of polarization vectors with different ferroelectric phases on (001) plane; M_A , M_B , and M_C are the different types of monoclinic phase, which can be considered as intermediate transition phases to connect two distinct ferroelectric phases. (c) Schematic illustration of polarization rotation evolution in tetragonal structure driven by the continuous shear strain δ_5 .

on the KNN cell. The evolutions of polarization rotation and shear piezoelectric constant are analyzed as a function of the shear strain. A direct relationship between piezoelectricity and polarization rotation will be revealed. The exchange-correlation functional is treated within the generalized gradient approximation parametrized by Perdew, Burke, and Ernzerhof [15]. The electron-ion potential is described by the projector augmented-wave method [16]. The polarization of KNN is rigorously defined by the so-called modern theory of polarization as proposed by Vanderbilt *et al.* [17–19], in order to eliminate the “improper” polarization quantum. Then the “proper” piezoelectric tensor can be calculated by $e_{\alpha j} = \partial P_{\alpha} / \partial \delta_j$ and does not suffer from any branch dependence. The composition of $K_{0.5}Na_{0.5}NbO_3$ is chosen to conduct the calculations, and the K and Na are randomly placed at the A site of the ABO_3 structure by the special quasirandom structure (SQS) approach [20]. The SQS approach has demonstrated its ability to capture the local structure accurately in the KNN system [21].

The three ferroelectric phases, rhombohedral, orthorhombic, and tetragonal in KNN crystal, whose polarization vectors can be only allowed to point in some isolated crystal orientations, such as $\langle 100 \rangle_{PC}$, $\langle 110 \rangle_{PC}$, and $\langle 111 \rangle_{PC}$, are shown in Fig. 1(a). However, Vanderbilt *et al.* deduced that an eight-order Devonshire theory allows for three kinds of low-symmetry monoclinic ferroelectric phases, M_A , M_B , and M_C , in perovskite structure [22], which enable themselves to rotate polarization on the $(\bar{1}10)_{PC}$, $(100)_{PC}$, and $(010)_{PC}$ planes, respectively. These monoclinic structures therefore can be considered to play an intermediate transition state and connect the two distinct ferroelectric phases, impelling the polarization rotation [22–24]. Specifically, as displayed in Fig. 1, the M_A , M_B , and M_C facilitate the rhombohedral-tetragonal, rhombohedral-orthorhombic, and

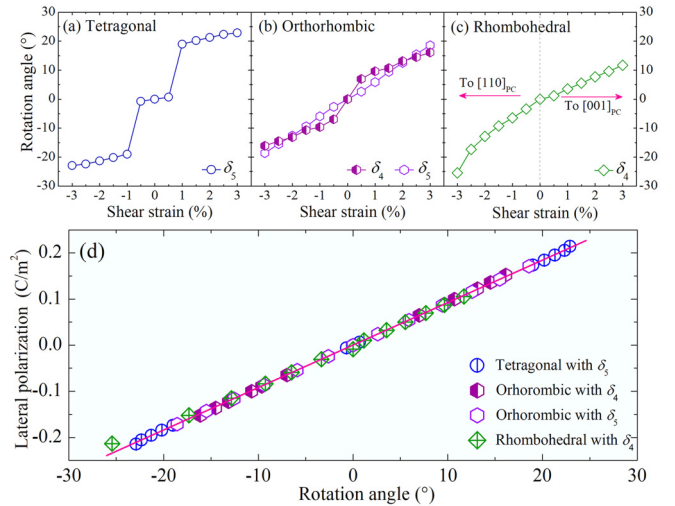


FIG. 2. (a)–(c) Rotation angle as a function of shear strain in three kinds of ferroelectric structure. (d) Direct linear correlation between lateral polarization and rotation angle.

orthorhombic-tetragonal polarization rotations, respectively. Due to the sensitivity of ferroelectricity originated from strong coupling between electrical polarization and elastic distortion in the perovskite structure, a T-O polarization tilting from $[001]_{PC}$ to $[101]_{PC}$ can be induced by applying a shear strain δ_5 on a tetragonal structure. As shown in Fig. 1(c), a series of successive strains δ_5 may cause the polarization rotation via an M_C -type monoclinic structure.

The shear piezoelectric effects of tetragonal, orthorhombic, and rhombohedral KNN are investigated to study the promotion of monoclinic structures on the polarization rotation, and the details can be found in Supplemental Material [25]. We show the polarization rotation angles as a function of shear strain in Figs. 2(a)–2(c), which exhibit the large rotation angle with these small shear strains. The steadily boosted polarization rotation indicates that it is possible to realize the ferroelectric phase transition via the intermediate monoclinic structure. The abrupt change of rotation angle around the strain of ± 0.01 in Fig. 2(a) originates from the low-energy phase transition from tetragonal to M_C structure. Another point to be noted is that rotation angle is asymmetric to shear strain in Fig. 2(c), which is because the positive δ_4 promotes polarization to $[001]_{PC}$ via M_A structure, but the negative δ_4 promotes polarization to $[110]_{PC}$ via M_B structure in our used supercell. The high-energy barrier of the tetragonal phase hinders the further polarization rotation to $[001]_{PC}$, leading to the smaller rotation angle. Figure 2(d) depicts the lateral polarization as a function of rotation angle, and there is a direct correlation between lateral polarization and rotation angle. The larger the polarization angle, the higher the lateral polarization. Moreover, the total polarizations under the application of shear strain do not show significant change [25], indicating the large lateral polarization mainly comes from the polarization rotation.

The energies for all possible ferroelectric phases in comparison with the cubic structure are investigated in Fig. 3(a). The large energy difference exhibits the nature of the unstable paraelectric state at low temperature, while the M_A ,

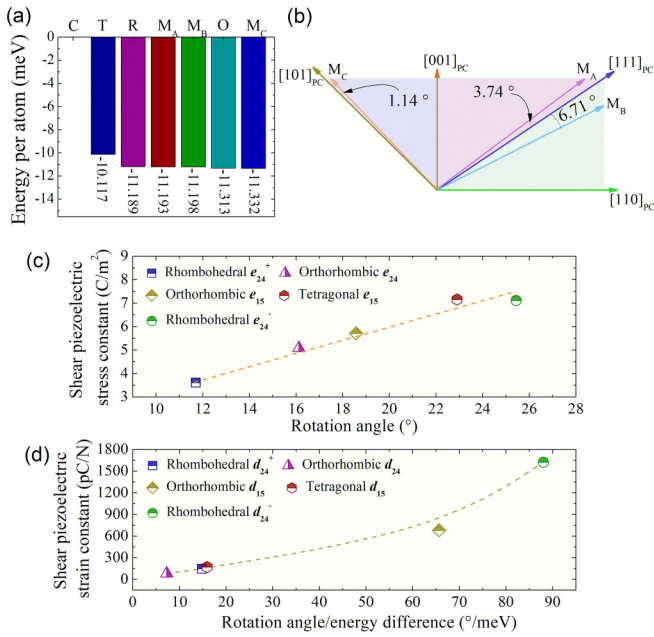


FIG. 3. (a) Energy for different ferroelectric and paraelectric phases; the energy difference is referenced to the cubic phase minima. C, T, O, and R represent the cubic, tetragonal, orthorhombic, and rhombohedral phase, respectively. (b) Schematic for three types of calculated monoclinic polarization. (c) Average shear piezoelectric stress constant vs rotation angle and (d) average shear piezoelectric strain constant vs rotation angle/energy difference under the shear strain of 0.03; because of the asymmetric change on the rhombohedral structure under the shear strain, $+$ and $-$ represent applying positive and negative strain, respectively.

M_B , and M_C have comparable energy with the R and O phases, exhibiting the possibility of coexistence between monoclinic and other ferroelectric phases. The results confirm the more energy-stable monoclinic structure at room temperature, M_C . However, the small angle of 1.14° between polarization vectors of M_C and O structures implies the non-significant difference of their lattice parameters, which leads to the indistinguishable phase in experiments. It must be noted that our calculated data give an inconsistent result in comparison with the experimental fact; here, the orthorhombic structure has lower energy than the rhombohedral one, but the experiment shows that the rhombohedral structure is the ground state [6–8]. As the end member of KNN, KNbO_3 with rhombohedral structure has the lowest energy in its possible structures confirmed by the first-principle method [31], whereas we do not find any other calculations to compare the energies of the orthorhombic and rhombohedral phases in the KNN system. However, the renewed phase diagram shows the rhombohedral-orthorhombic transition temperature gradually decreases to ~ 50 K with the rise of Na content in the range of 0 to 0.5 [8], suggesting the small energy difference between orthorhombic and rhombohedral structures in KNN. Besides, the energetically favorable phase may be connected to the atomic order of A site. Depending on the cation order, different tilt systems are energetically favorable in $\text{Bi}_{0.5}\text{Na}_{0.5}\text{TiO}_3$, which has been demonstrated by the previous first-principles simulation work [32,33]. Our result reveals that the energies

of M_A , M_B , and M_C are close to those of rhombohedral and orthorhombic structures; thus, they can act as a second-order transitional bridge to connect these ferroelectric phases. This fact can in principle result in a strong piezoelectric response. With the rise of temperature, it can be expected that the free energies of two ferroelectric phases are equal and the energy surface is further flat on the polarization connection path near the ferroelectric phase boundary, which strongly facilitates the continuous rotation of polarization via these monoclinic structures.

We use linear fitting to compute the average shear piezoelectric stress constant under the shear strain of 0.03, which is plotted as a function of rotation angle in Fig. 3(c) to elucidate the relationship between rotation angle and piezoelectric stress constant. A strongly linear correlation between rotation angle and shear piezoelectric stress is presented. The rhombohedral e_{24}^- is divided into two parts because of different changes in polarization and energy for applying positive and negative shear strain, which are represented by the superscripts “ $+$ ” and “ $-$ ”, respectively. These shear piezoelectric stress constants are significantly different. The rhombohedral e_{24}^- and tetragonal e_{15} are more than 7 C/m^2 , which are almost twice that of rhombohedral e_{24}^+ . Figure 3(c) displays a direct correlation between the shear piezoelectric stress constant and rotation angle, with the larger polarization rotation angle conforming to higher piezoelectric stress constant. Such a fact supports that the shear piezoelectric response mainly comes from the polarization rotation induced by applied stress or electric field in the lead-free system, in which the near-energy intermediate monoclinic structure may play a critical role for continuous rotation behavior.

As a typical displacive ferroelectric, the polarization rotation of KNN is evoked by internal microscopic ionic relaxations in response to a macroscopic shear strain. To understand the atomic origin of high-shear piezoelectric constants, the piezoelectric stress constant should be decomposed into two parts [34],

$$e_{\alpha j} = \left. \frac{\partial P_\alpha}{\partial \delta_j} \right|_u + \sum_k \frac{ec}{\Omega} Z_{k,\alpha\alpha}^* \frac{\partial u_{k,\alpha}}{\partial \delta_j}, \quad (1)$$

where P is the polarization, δ is the strain, the k runs over the whole atoms in the cell of volume Ω , e is the electron charge, c is the lattice parameter along the polar vector, $Z_{\alpha\alpha}^*$ is the Born effective charge, and u is the internal atomic coordinate. In Eq. (1), the first part is the frozen-ion term and represents the piezoelectric constant without internal atomic relaxation. The second part is the internal-strain term and represents the contributions of ionic relaxation for the piezoelectric constant. The internal-strain term dominates the total piezoelectric response in inorganic perovskite ferroelectrics, such as BaTiO_3 , PbTiO_3 , KNbO_3 as well as $\text{K}_{0.5}\text{Na}_{0.5}\text{NbO}_3$ [11,34–37]. From Eq. (1), the internal-strain term strongly depends on the Born effective charge and the coupling of internal coordinates with applied strain. The Born effective charges of Nb and O are totally much larger than their nominal charges [25], suggesting that the ferroelectricity of KNN is driven by the chemical bonding effect. The large Born effective charge, as well as high response of internal atomic

coordinate to the macroscopic shear strain, indicates shear piezoelectric constant mainly comes from the displacement change of Nb and O, while the K atom plays a nonsignificant role in this process [25]. However, the contribution of Na with the almost same Born effective charge of K, cannot be neglected; its responses of internal coordinates are 3–4 times that of Nb in orthorhombic and rhombohedral structures and even 5–9 times that of Nb in tetragonal structure, which are considerable for piezoelectric stress constant.

The piezoelectric strain constant is more commonly discussed in the experiments. To accurately define the average rhombohedral d_{24}^+ and d_{24}^- , the curves of energy under the condition of positive and negative δ_4 are refitted and the c_{44}^+ and c_{44}^- are computed as 26.09 and 15.78 GPa, respectively. Figure 3(d) shows the rhombohedral d_{24}^- is as high as 1624 pC/N, which can be attributed to the coupling of high polarization rotation and soft lattice deformation. Although the average orthorhombic e_{15} of 5.709 C/m² is inferior to the tetragonal one, the orthorhombic d_{15} is over 400% larger than the tetragonal one due to the extremely low c_{55} of 8.41 GPa in orthorhombic structure. We check the force-response internal-strain tensor of orthorhombic KNN and find that O-Nb-O chains in $[100]_{\text{PC}}$ and $[001]_{\text{PC}}$ directions have an almost full contribution for softening of c_{55} . Such low c_{55} may be derived from the nearby low-energy M_C structure, which has been reported in some experiments and is considered to be close to orthorhombic crystal structure [8,38]. It is the susceptibility of the structure to M_C distortion that is the underlying mechanism of the enhancement. Another point is noted that both the orthorhombic d_{24} and rhombohedral d_{24}^+ are less than 150 pC/N. In such cases, polarization is induced to rotate towards the higher-energy phase; therefore, the high-energy barrier prevents further rotation and leading to an inferior piezoelectric response. Nevertheless, the shear piezoelectric strain constant is still much higher than the longitudinal piezoelectric constant, $d_{33} \sim 29.1$ pC/N [11]. Figure 3(d) exhibits the correlation of piezoelectric strain constant and polarization rotation/energy difference, which is following the results of the Landau-Ginsburg-Devonshire phenomenological theory [39] and the first-principles constrained polarization molecular-dynamics simulation [40]. The readily impellent polarization rotation with strong polarization fluctuation drives up the dielectric susceptibility and thus enhances the piezoelectric response.

The experimental results indicate that the coexistence of rhombohedral and tetragonal structures results in the highest piezoelectric response in modified KNN ceramics [9], whereas our first-principle calculations show that rhombohedral structure via M_A -type polarization rotation realizes a small rotation angle and an inferior d_{24}^+ . This is because of the huge energy difference between rhombohedral and tetragonal phases in undoped KNN at 0 K, which hinders the high piezoelectricity. In our view, polarization rotation in fact still supports that the coexistence of rhombohedral and tetragonal structures will give rise to high piezoelectricity intrinsically because it has a higher theoretical maximum polarization rotation angle of 54.74° than M_B and M_C -type polarization rotation, and thus large polarization change in nonpolar directions as long as the M_A -type rotation occurs. With the rise of

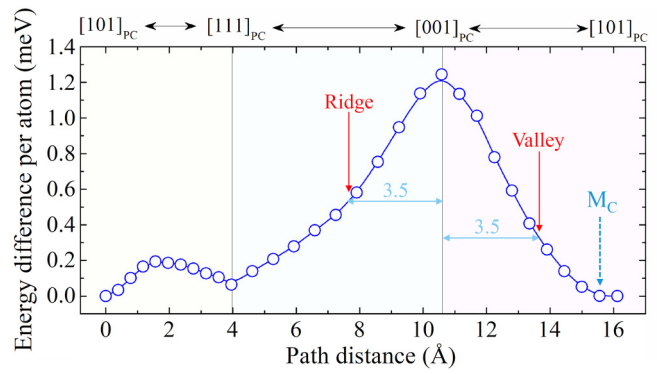


FIG. 4. Energetics for polarization rotation. The nudged elastic band method is used to calculate the nine images for each path. The path distance is the distance between the intersections of the polarization vectors on the $(001)_{\text{PC}}$ plane, as shown in Fig. 1(b).

temperature, the thermotropic ferroelectric phase boundary is expected to decrease the energy barrier. Moreover, it should be noted that the presence of monoclinic phases is instrumental in the flattening of the free-energy profile, in which under the application of stress or electric field, the ferroelectric phase deforms along a monoclinic path easily [34]. In such a case, the magnitude of polarization rotation angle will be critical to determine the piezoelectric strain constant. However, we have to point out the direct M_A -type polarization may not occur in the lead-free system. In a thermotropic R-T or R-O-T phase transition, which widely exists in high-performance KNN-based ceramics [9,10,41], the O phase may play a critical role to construct the connection between R and T. In the same path distance in Fig. 4, the energy of the O-T path is lower than that of R-T, suggesting the O-T path is the valley of the energy landscape. This valley in Fig. 4 is formed from the path that connects the perovskite-derived global energy minimum, M_C structure. Since the elastic stiffness constant is the curvature of the total energy with respect to strain, the existence of a Gibbs free-energy flattening eases the phase transformation via the valley, which is demonstrated in Fig. S4(a) [25]. Therefore, instead of a direct R-T transition, the polarization is more likely to rotate along the R- M_B -O- M_C -T path in such a case. The recent reports actually have realized the KNN-based ceramics with high piezoelectricity is the structure of the coexistence of R, O, and T instead of past R and T [10,42]. However, the critical role of the O phase should be further indicated. The further experimental study should focus on the broad temperature-dependent phase transition region in high-performance KNN-based materials and giving straightforward evidence for the speculation.

In summary, the first-principles calculations are performed to study the origin of high-shear piezoelectric response in the lead-free KNN system. The detailed evolution of shear strain-induced polarization rotation has been demonstrated in the present work, and the continuous polarization rotation via the intermediate monoclinic structure is revealed. A direct correlation between polarization rotation and shear piezoelectric constant is found. The higher the polarization rotation angle and flatter the energy surface, the larger the piezoelectric shear piezoelectric constant. The atomic insight indicates the

polarization rotation can be mainly ascribed to the reorientation of Nb and O atoms under the external field, and Na plays a considerable role for shear piezoelectricity due to its highest response of internal coordinate to macroscopic strain. Our results support the classical R-T phase boundary could produce high piezoelectricity in principle. However, we suggest that instead of a direct R-T rotation path, the R-M_B-O-M_C-T transition is more likely to be adopted in modified KNN-based materials with wide temperature-dependent thermotropic R-T or R-O-T phase boundary. We hope that this work will inspire

future experimental studies for further developing lead-free piezoelectric materials.

The authors gratefully acknowledge the support of the National Natural Science Foundation of China (Grants No. 52032007, No. 12004267, and No. 51932010), the R & D Projects in Key Fields of Guangdong Province, China (Grant No. 2020B0109380001), and the Fundamental Research Funds for the Central Universities of China (Grants No. 2020SCU12001 and No. 2021SCU12058).

-
- [1] K. Uchino, *Piezoelectric Actuators and Ultrasonic Motors* (Kluwer Academic, Boston, 1996).
- [2] M. A. Akbas and P. K. Davies, *J. Am. Ceram. Soc.* **81**, 670 (1998).
- [3] B. Jaffe, W. R. Cook, and H. Jaffe, *Piezoelectric Ceramics* (Academic Press, London, 1971).
- [4] Y. Saito, H. Takao, T. Tani, T. Nonoyama, K. Takatory, T. Homma, T. Nagaya, and M. Nakamura, *Nature (London)* **432**, 84 (2004).
- [5] P. Li, J. Zhai, B. Shen, S. Zhang, X. Li, F. Zhu, and X. Zhang, *Adv. Mater.* **30**, 1705171 (2018).
- [6] V. J. Tennery and K. W. Hang, *J. Appl. Phys.* **39**, 4749 (1968).
- [7] M. Ahtee and A. M. Glazer, *Acta Cryst.* **32**, 434 (1976).
- [8] D. W. Baker, P. A. Thomas, N. Zhang, and A. M. Glazer, *Appl. Phys. Lett.* **95**, 091903 (2009).
- [9] J. Wu, D. Xiao, and J. Zhu, *Chem. Rev.* **115**, 2559 (2015).
- [10] H. Tao, H. Wu, Y. Liu, Y. Zhang, J. Wu, F. Li, X. Lyu, C. Zhao, D. Xiao, J. Zhu, and S. J. Pennycook, *J. Am. Chem. Soc.* **141**, 13987 (2019).
- [11] Z. Tan, Y. Peng, J. An, Q. Zhang, and J. Zhu, *J. Am. Ceram. Soc.* **102**, 5262 (2019).
- [12] M. Davis, M. Budimir, D. Damjanovic, and N. Setter, *J. Appl. Phys.* **101**, 054112 (2007).
- [13] G. Kresse and J. Hafner, *Phys. Rev. B* **49**, 14251 (1994).
- [14] G. Kresse and J. Furthmüller, *Phys. Rev. B* **54**, 11169 (1996).
- [15] J. P. Perdew, K. Burke, and M. Ernzerhof, *Phys. Rev. Lett.* **77**, 3865 (1996).
- [16] P. E. Blöchl, *Phys. Rev. B* **50**, 17953 (1994).
- [17] R. D. King-Smith and D. Vanderbilt, *Phys. Rev. B* **47**, 1651(R) (1993).
- [18] R. Resta, *Europhys. Lett.* **22**, 133 (1993).
- [19] D. Vanderbilt and R. D. King-Smith, *Phys. Rev. B* **48**, 4442 (1993).
- [20] A. van de Walle, P. Tiwary, M. de Jong, D. Olmsted, M. Asta, A. Dick, D. Shin, Y. Wang, L.-Q. Chen, and Z.-K. Liu, *Calphad* **42**, 13 (2013).
- [21] B. K. Voas, T. M. Usher, X. Liu, S. Li, J. L. Jones, X. Tan, V. R. Cooper, and S. P. Beckman, *Phys. Rev. B* **90**, 024105 (2014).
- [22] D. Vanderbilt and M. H. Cohen, *Phys. Rev. B* **63**, 094108 (2001).
- [23] N. Huang, Z. Liu, Z. Wu, J. Wu, W. Duan, B. L. Gu, and X. W. Zhang, *Phys. Rev. Lett.* **91**, 067602 (2003).
- [24] L. Bellaïche, A. García, and D. Vanderbilt, *Phys. Rev. B* **64**, 060103(R) (2001).
- [25] See Supplemental Material at <http://link.aps.org/supplemental/10.1103/PhysRevB.104.014104> for detailed supercell information, polarization evolution, energetics as a function of strain, elastic tensor, lateral Born effective charge, and internal atomic coordinate change, which includes Refs. [11] and [26–31].
- [26] R. Zhang, B. Jiang, and W. Cao, *Appl. Phys. Lett.* **82**, 787 (2003).
- [27] F. Li, S. Zhang, Z. Xu, X. Wei, and T. R. Shrout, *Adv. Funct. Mater.* **21**, 2118 (2011).
- [28] L. Wu, J. L. Zhang, C. L. Wang, and J. C. Li, *J. Appl. Phys.* **103**, 084116 (2008).
- [29] A. G. Kalinichev, J. D. Bass, C. S. Zha, P. D. Han, and D. A. Payne, *J. Appl. Phys.* **74**, 6603 (1993).
- [30] M. Zgonik, R. Schlessler, I. Biaggio, E. Voit, J. Tscherry, and P. Gunter, *J. Appl. Phys.* **74**, 1287 (1993).
- [31] L. F. Wan, T. Nishimatsu, and S. P. Beckman, *J. Appl. Phys.* **111**, 104107 (2012).
- [32] J. A. Dawson, H. Chen, and I. Tanaka, *J. Mater. Chem. A* **3**, 16574 (2015).
- [33] F. Pforr, K. C. Meyer, M. Major, K. Albe, W. Donner, U. Stuhr, and A. Ivanov, *Phys. Rev. B* **96**, 184107 (2017).
- [34] X. Wu, D. Vanderbilt, and D. R. Hamann, *Phys. Rev. B* **72**, 035105 (2005).
- [35] G. Sági-Szabó, R. E. Cohen, and H. Krakauer, *Phys. Rev. Lett.* **80**, 4321 (1998).
- [36] L. Bellaïche and D. Vanderbilt, *Phys. Rev. Lett.* **83**, 1347 (1999).
- [37] Y. Peng, Z. Tan, J. An, J. Zhu, and Q. Zhang, *J. Eur. Ceram. Soc.* **39**, 5252 (2019).
- [38] J. Tellier, B. Malic, B. Dkhil, D. Jenko, J. Cilensek, and M. Kosec, *Solid State Sci.* **11**, 320 (2009).
- [39] D. Damjanovic, *J. Am. Ceram. Soc.* **88**, 2663 (2005).
- [40] A. Kumar, K. M. Rabe, and U. V. Waghmare, *Phys. Rev. B* **87**, 024107 (2013).
- [41] M. H. Zhang, K. Wang, Y. J. Du, G. Dai, W. Sun, G. Li, D. Hu, H. C. Thong, C. Zhao, X. Q. Xi, Z.-X. Yu, and J.-F. Li, *J. Am. Chem. Soc.* **139**, 3889 (2017).
- [42] J. Fu and R. Zuo, *Acta Mater.* **195**, 571 (2020).